Impact of industrially applied surface finishing processes on tribocorrosion performance of 316L stainless steel

Stephania Kossman [a,*], Leonardo B. Coelho [b], Alberto Mejias [a], Alex Montagne [a], Adrien Van Gorp [a], Thierry Coorevits [a], Matthieu Touzin [c], Marc Poorteman [b], M.-G. Olivier [b], Alain Iost [a], Mariana H. Staia [a,d]

[a] *Arts et Metiers Institute of Technology, MSMP, HESAM Université, 8 Boulevard Louis XIV, 59000, Lille Cedex, France*
[b] *Department of Materials Science, Faculty of Engineering, University of Mons, 20 Place du Parc, 7000, Mons, Belgium*
[c] *Univ. Lille, CNRS, INRAE, ENSCL, UMR 8207 - UMET - Unité Matériaux et Transformations, F-59000, Lille, France*
[d] *Escuela de Ingeniería Metalúrgica y Ciencia de los Materiales, Facultad de Ingeniería, Universidad Central de Venezuela, Caracas, Venezuela*

ARTICLE INFO

ABSTRACT

This investigation addresses the effect provided by industrial surface finishes on the tribocorrosion properties of 316L stainless steel exposed to NaCl solution. Three distinct surface treatments were evaluated: passivation (SSO), electropolishing-passivation (SSEP) and micro-undulation (SSM mechano-chemical + electropolishing + passivation). For the tribocorrosion tests, a potentiostatic approach was considered in order to highlight the alloy behavior under two opposite situations, where repassivation of the surface would be thermodynamically possible or not (anodic or cathodic polarization, respectively). The outcomes demonstrated that the surface treatments were either harmful (SSEP) or beneficial (SSM) in terms of resulting tribocorrosion resistance. The specific topography of the micro-undulated sample decreased the real contact area and improved the surface lubrication in aqueous medium. SSEP presented the highest chemical wear and several factors seemed to have contributed for it, including the chemical, mechanical and structural properties of the passive film. Regardless the surface treatment, the tribocorrosion response was modified by the applied potential and more severe damage was determined under anodic polarization. At this potential, calculations of the total surface degradation suggested that volume loss was mainly dominated by chemical wear.

1. Introduction

Stainless steels are well known for their high corrosion resistance credited to the formation of a rich chromium oxide layer on the surface (passive layer), and therefore, frequently represent an appropriate material alternative for applications in corrosive environments. Moreover, stainless steel parts are often submitted to the combination of corrosion and wear in several industry sectors such as pharmaceutical, food processing, biomedical, power generation, etc.

The degradation of stainless steels is related to the deterioration and breakdown of the passive layer, either by mechanical damage (*e.g.* wear), corrosion action (*e.g.* pitting) or the combination of both (*e.g.* tribocorrosion). The so-called tribocorrosion process involves material degradation induced by the simultaneous action of corrosion and wear. Although the process substantially impacts the material surface, the

mechanical properties at the subsurface could also be affected due to hydrogen evolution and absorption phenomena [1]. Both processes contributing to tribocorrosion are coupled, as corrosion may modify the friction conditions (*e.g.* due to corrosion products on the contact surface), while friction and wear can render the material sensitivity to corrosion (*e.g.* removal of the passive layer by wear). The basic mechanism of the tribocorrosion response of passive alloys consists in the disruption of the passive layer by wear action, which produces an active area, causing metal oxidation and dissolution until repassivation eventually occurs. In real life applications, these actions often occur periodically, producing repeated depassivation-repassivation steps that lead to a synergy between mechanical stresses and environmental effects, thus resulting in premature damage due to accelerated loss of functionality [1,2]. The tribocorrosion behavior of passive materials in general, and of stainless steels in particular, has been largely studied

during the last decades, with particular attention paid to the interaction and synergism of wear and corrosion. These phenomena are so diverse and complex that they were not yet fully elucidated to date [3–7].

Several factors interfere in the corrosion, wear and tribocorrosion response of stainless steels. Among them, the nature of the passive film (structure and chemical composition [8–13]) and the surface topography (roughness and real surface area [7,12,14,15]) play a significant role. These two factors could be modified by surface finishing treatments, which are mainly applied to improve the characteristics of the passive layers and the surface roughness according to target purposes [12,16,17].

Considering industrial applications, stainless steel surfaces are typically treated to improve their corrosion resistance by pickling and/or passivation (chemical treatments) or by electropolishing (electrochemical process). Pickling and passivation have a lower cost than electropolishing and are based on the dissolution of low corrosion resistant phases/impurities by controlled acidic attack, thus increasing the overall anti-corrosion properties [18–20]. By comparison, electropolishing is applied, not only to enhance the corrosion resistance, but also to reduce surface roughness. Electropolishing prompts preferential dissolution reactions in an electrolyte upon the application of anodic currents, producing a uniform Cr-rich passive layer, the dissolution of the strained layer and a lower roughness with a brilliant surface [21,22]. This more expensive alternative is claimed as cost effective over time [23].

Moreover, mechanical resistance and fatigue life of stainless steels could be improved by surface finishing treatments such as severe plastic deformation (SPD) processes (*e.g.* shot peening, surface mechanical attrition (SMAT)). The principle of these treatments consists in a shot stream blasted against the metallic surface [24], inducing heavy straining of the surface under high pressure and microstructural modifications, which could enhance the physical, mechanical and chemical properties [25,26].

The effect of the surface finishing treatments on the corrosion resistance of stainless steels has been investigated for years [12,27–30]. However, from a tribocorrosion point of view, considerable less literature is available [31]. Nonetheless, it is well known that under tribocorrosion solicitations the surface properties affect both wear and electrochemical responses, notably the friction coefficient and the surface reactivity [2]. Likewise, the chemistry of the passive layers modifies the wear-corrosion response, eventually leading to the arise of galvanic coupling [5]. Moreover, surface hardness modifications also alter the tribocorrosion behavior. Literature models [3,4] propose that the anodic current varies inversely proportional to the material hardness. Sun and Bailey work [32] clearly showed an evidence of this behavior as the stainless steel surface treated by SMAT (inducing a higher hardness) presented less mechanical and chemical wear.

With this background in mind, this study is a first effort to address the wear and tribocorrosion properties of 316L stainless steel (316LSS) surfaces presenting three industrial surface finishes, namely: passivation, electropolishing-passivation and micro-undulation (mechanochemical + electropolishing + passivation). The micro-undulation technology [33] is claimed to produce superior tribocorrosion behavior, particularly in systems susceptible to wear-corrosion solicitations. The tribocorrosion studies here presented were a necessary step, after a preliminary electrochemical/mechanical investigation, for demonstrating the difference among the substrates, in terms of their surface, mechanical and corrosion properties [34]. The results here obtained show that the industrial surface treatments indeed modified the tribocorrosion response of 316L in NaCl media, producing either detrimental (when electropolishing is applied) or positive (in case of micro-undulation) effects.

2. Materials and methodology

2.1. Materials

The investigated materials were 316L stainless steel plates (Aperam, France) subjected to three distinct industrial surface treatments (Packo Inox nv, Belgium). The employed nomenclature and the processes implicated in the three surfaces treatments are described below. The same materials and corresponding nomenclature were employed in a previous investigation of some of the authors prior to this one [34].

- SSO: chemical passivation (the reference surface).
- SSEP: electropolishing followed by passivation. The electropolishing process was performed at 65 °C; and applied current densities varied between 20 and 40 A/dm^2.
- SSM: micro-undulation followed by electropolishing and passivation. The micro-undulation treatment (mechanochemical procedure) comprises a severe plastic deformation process (*e.g.* shot peening or SMAT) combined with acidic etching. This last step produces a micro-roughness topography, which is locally decreased in a controlled way by electropolishing.

The initial surface state of all plates was 2B surface finish (cold rolling, annealing, pickling and light skin cold rolling) [35,36]. As previously mentioned, the three surfaces were passivated as a last step before final water rinsing, using an acid solution including nitric acid. This step is intended to produce surfaces with even higher corrosion resistance. It is worth mentioning that the authors do not dispose of further technical information about the treatments due to the industrial confidentiality agreements.

The bulk composition of the 316L specimens is very similar, regardless of the surface treatment. The average composition in wt% is: Cr 17.3, Ni 10.1, Mo 2.2, Cu 0.5, Mn 0.3, Si 0.2, C 0.02-0.03, Fe balance [34]. Nonetheless, the passive layers of SSEP and SSM samples presented chromium enrichment. The thicknesses of the passive films are about 4 nm for the three types of surface [34].

The specimen microstructures presented variations depending on the applied surface treatment [34]. It was reported [34] that SSO exhibited a grain-like microstructure typically observed in 2B surface finishing. Meanwhile the SSEP samples showed a grain-like microstructure presenting twinned grains, characteristic of austenitic stainless steels. However, in the case of the SSM sample, a grain-like microstructure with an important degree of twinning was determined, which is usually observed in surfaces treated by shot peening or SMAT.

Mechanical properties (elastic modulus and hardness) were determined in a preliminary work [34]. As expected, the elastic modulus was constant regardless the surface treatment (approximately 195 GPa). Nevertheless, hardness was increased due to the micro-undulation process, reaching 3.6 GPa (representing about 71% of increase with respect to SSO and SSEP).

Surface morphology parameters (roughness and waviness), are reported elsewhere [34] revealed an effective decrease in roughness after electropolishing and a significant increase in this as induced by micro-undulation treatment (*e.g.* R_t equals to 2.4, 1.1 and 6.6 μm for SSO, SSEP and SSM, respectively).

2.2. Wear and tribocorrosion tests

2.2.1. Wear tests (dry)

The wear tests were performed in a pin-on-disc tribometer TRIBO-tester (Tribotechnic, France) using an alumina ball of 10 mm diameter (grade 25, ISO 3290) as counterpart. The tests were carried out at two normal loads of 1 and 5 N, respectively corresponding to the approximate maximum contact pressures of 548 and 937 MPa. The sliding distance was 10 m (equivalent to ~800 cycles) for a sliding rate of 12.6 mm/s (60 rpm) and a wear track radius of 2 mm. The contact interval

time was 1000 ms. All tests were performed at room temperature (22 °C) and triplicated for reproducibility.

2.2.2. Tribocorrosion tests

Corrosion measurements were performed using a typical three electrode configuration: 316LSS as working electrode (WE) (exposed area of 1.76 cm^2 properly isolated), an Ag/AgCl/KCl$_{sat}$ as reference electrode (RE) and a Pt-wire auxiliary electrode. The electrolyte used was aqueous 0.5 M NaCl and the working solution volume was maintained constant (35 ml) for all experiments. The corrosion measurements were done using a potentiostat/galvanostat Solartron 1287 (Ametek, USA). The tribocorrosion tests were performed using an original home-made cell conceived for this study and fabricated by 3D printing (details are given in the supplementary material), which improved tests reproducibility regarding the mounting conditions of the three electrodes configuration.

The tests were carried out under potentiostatic control at cathodic and anodic potentials selected from previously studied potentiodynamic polarization curves [34]. The corresponding cathodic and anodic potentials were: E_{cat} = –400 mV and E_{pass} = +200 mV vs. Ag/AgCl/KCl$_{sat}$. The anodic potential chosen (E_{pass}) corresponds to well-defined passivity ranges observed for all surfaces. This potentiostatic approach was selected to evaluate the tribocorrosion behavior of the 316L samples in two clearly distinct situations, in which passive layers could be - or not - spontaneously formed on the surfaces. The tribocorrosion testing under cathodic potential could be considered as a "pure wear" experiment if the following conditions are satisfied: (1) the applied E_{cat} is low enough for the working electrode to be under cathodic protection (absence of corrosion); (2) the oxygen reduction reaction is the main cathodic process at E_{cat} (water reduction reaction and associated hydrogen evolution could lead to hydrogen embrittlement [37]).

Wear measurements during tribocorrosion tests were conducted under the same conditions described above for dry wear testing. During the tribocorrosion tests, the current (I) and the coefficient of friction (COF) were recorded simultaneously.

2.2.3. Wear tracks characterization

The post-mortem characterization of wear tracks was performed by scanning electron microscopy (SEM) (Hitachi S-520, Japan), SEM coupled with energy-dispersive X-ray spectroscopy (EDS) (JEOL JSM-7800F LV, Japan) and optical profilometry (Veeco NT-9300, USA). The alumina balls counterparts were characterized by optical profilometry after tribocorrosion tests.

The wear track volumes were estimated from optical profilometry measurements done at eight uniformly distributed locations along the wear track circumferences. These profiles were taken perpendicularly to the sliding track. Then, the cross-section areas A of the wear tracks were calculated utilizing the software Mountains®7 (Digital Surf, France). Therefore, the average A is multiplied by the perimeter of the wear track circumference to obtain the total volume loss (V_t).

In order to determine possible work hardening after tribocorrosion tests, such as reported in the literature [38,39], nanoindentation tests were carried out on the wear tracks obtained at 5 N, according to previous experimental settings described elsewhere [34].

3. Assessment of material degradation during tribocorrosion tests

The total degradation of the material during tribocorrosion tests can be described by a simple mechanistic model (Eq. (1)) [40], which considers that material deterioration results from mechanical wear and chemical wear:

$$V_t = V_{mech} + V_{chem} \tag{1}$$

where V_t is the total tribocorrosion material loss, V_{mech} is the material

mechanically removed by wear, and V_{chem} is the material loss due to corrosion, also called chemical wear.

The chemical wear was calculated by Faraday's law (Eq. (2)), assuming that the current flows mainly through the wear track during the tribocorrosion test (at anodic potential, E_{pass}). Hence, the material loss due to corrosion at passive potential without the action of rubbing was considered as negligible.

$$V_{chem} = \frac{ItM}{nF\rho} \tag{2}$$

where t is the sliding time, I is the average current during sliding flowing through the wear track surface, M is the atomic mass of the alloy given by $\sum X_i M_i$, where X_i is the mole fraction and M_i the atomic mass of the alloy constituents (materials section). F is the Faraday's constant (96485 C mol^{-1}), ρ is the material density (7.95 g cm^{-3}), and n is the valence of dissolution and oxidation that depends on the involved anodic reactions. Here it was assumed n = 2.5, supposing that active dissolution and passive oxidation occurred simultaneously during tribocorrosion tests [37].

The V_t parameter was measured by optical profilometry of the wear track as explained in section 2.2.3. At E_{pass}, V_{mech} was obtained by the difference between V_t and V_{chem}. At E_{cat}, $V_{mech} = V_t$ since damage was considered to occur only by mechanical wear at this potential [37].

4. Results

4.1. Wear: pin-on-disc tests in dry conditions

Before studying tribocorrosion, pin-on-disc tests were performed under dry conditions either using normal loads of 1 or 5 N. The evolution of friction coefficients is presented in Fig. 1. One representative curve is shown for each surface state for illustrative purpose, however all curves for each surface state presented a similar trend.

The evolution of the friction coefficient (Fig. 1) showed an initial run-in period of about 200 cycles at 1 N and of around 20 cycles at 5 N, for all samples. After this period, especially at 1 N, the three samples presented fluctuations due to the complex mechanisms during the contact. The increase of the friction coefficient after the run-in period could be related to adhesion mechanisms. The decrease of COF as typically observed for SSM at 1 N could indicate the brief roughing out of the sample surface. However, a further increase of COF after these previous stages might be correlated to both the adhesion mechanism and the generation and entrapment of new particles [41], such as observed for SSEP at 1 N. The steady state was reached only at 5 N, after approximately 300 cycles, which was the result of a smoother contact surface due to the higher applied load.

Wear mechanisms were identified by means of SEM observations of the wear tracks. Adhesive wear was the main interaction mechanism identified on the wear tracks regardless the surface treatment. An example of the wear track morphology for the SSO surface, obtained at 1 N, is presented in Fig. 2. The features observed for SSO were also representative for SSEP and SSM, thus indicating that the friction response was practically independent of the surface roughness [42]. A 3D topography image is displayed next to the SEM images (Fig. 2c). Similar wear mechanism, *i.e.* adhesive wear was observed at 5 N as well (images not provided here). A comparable response was achieved by Sun [16] working under dry sliding conditions: no remarkable differences were found between non-treated and SMAT treated 304 stainless steel surfaces.

The alumina counterbody surfaces presented significant material accumulation (evaluated by optical profilometry) without presenting measurable wear regardless the characteristics of the tested steel surfaces. This response is typically obtained for this kind of tribological pair (hard ceramic against soft metal in air), in which a strong adhesive mechanism often prevails.
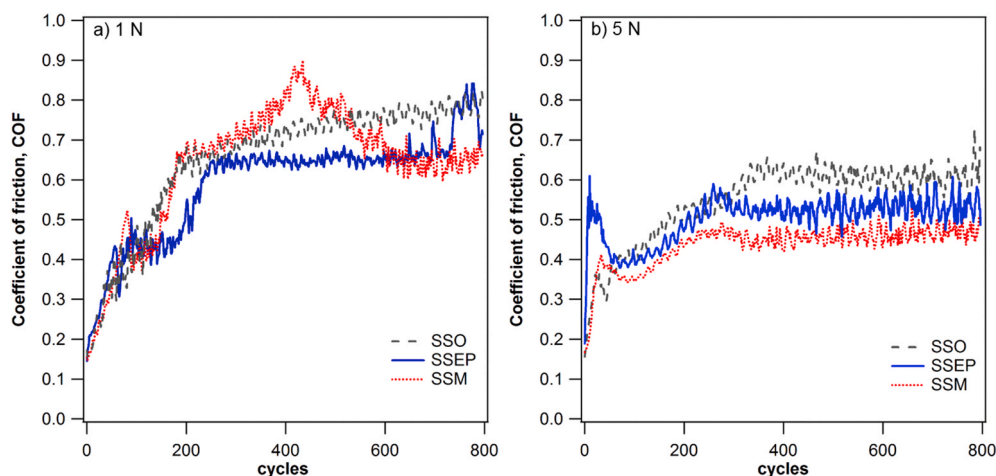
Fig. 1. Evolution of the coefficient of friction from pin-on-disc tests on stainless steel plates presenting different surface treatments (SSO, SSEP, SSM), the total testing time was approximately 800 s ≡ 800 cycles: a) 1 N and b) 5 N of normal load. (color online). (For interpretation of the references to color in this figure legend, the reader is referred to the Web version of this article.)
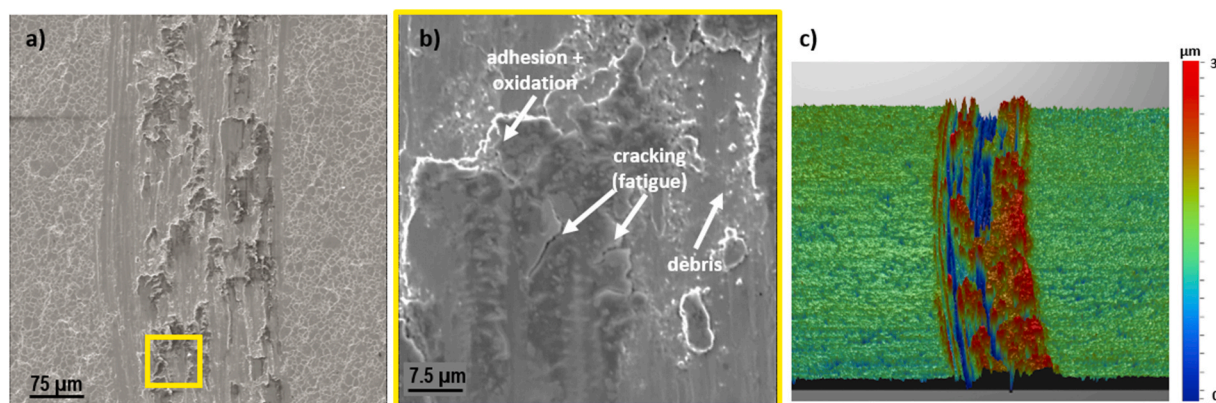
Fig. 2. Wear track morphology analysis of SSO after pin-on-disc tests (dry) at 1 N: a) SEM image (secondary electron mode) of the wear track; b) zoom of the framed area in (a); c) optical profilometry showing the strong adhesion. (color online). (For interpretation of the references to color in this figure legend, the reader is referred to the Web version of this article.)

The studied tribological pair led to an extensive plastic deformation of the surface asperities and subsequent displacement/adhesion of the soft metal onto the alumina ball. Moreover, the affinity of such alloy (oxidized surfaces) to oxygen would produce more adhesion to the ceramic counterpart [43]. Furthermore, the local-instantaneous high temperatures at the asperities could produce thermal oxidation, *i.e.* the flash temperature could be several orders of magnitude higher than the average temperature on the contact area [44,45].

In general, the adhered metal is brought back to the contact during the cyclic sliding, leading to more deformation. Throughout this process, wear debris (third body particles) are produced due to cracking during the fatigue process (Fig. 2b). Some of these debris are ejected from the contact zone resulting in wear loss, while others are retained within the contact, being agglomerated/compacted on the surface due to adhesion forces, creating new harder surface layers that could favor the protection of the surface [46]. These compacted layers can fracture producing more wear or can undergo sintering/cold-welding between particles, leading to the consolidation of the layers (darker regions within the wear track in Fig. 2a) [41,47,48].

The compacted layers observed in the wear tracks due to the adhesive mechanisms (Fig. 2a) hindered the estimation of the volume loss by means of optical profilometry (Fig. 2c). Hence, only the wear track widths obtained after testing at 1 N and 5 N are reported in Table 1.

The wear track width measurements indicated a significant lower

Table 1
Wear track width obtained from pin-on-disc tests (dry) at 1 and 5 N rubbing against alumina ball during 800 cycles.

	Width (μm) 1 N	Width (μm) 5 N
SSO	260 ± 24	460 ± 79
SSEP	206 ± 10	461 ± 52
SSM	181 ± 23	319 ± 29

wear volume for SSM at both testing loads. This fact could be related to the higher hardness of SSM (about 71% higher than SSO or SSEP) [34], in accordance with the classical Archard's wear law [49], which indicates that the amount of wear is proportional to the applied load/-sliding distance and inversely proportional to the material hardness. At 1 N, the wear damage of SSEP surface was reduced (narrower wear track) in comparison with SSO. Such a kind of response could be related to its low surface roughness and possible less plastic deformation, which vanished at 5 N due to a higher contact pressure.

4.2. Tribocorrosion: pin-on-disc tests in 0.5 M NaCl solution

The results obtained from tribocorrosion tests under potentiostatic control at $E_{pass} = +200$ mV and $E_{cat} = -400$ mV (vs. Ag/AgCl/KCl$_{sat}$), were evaluated to elucidate the particular behavior of SSO, SSEP and

SSM surface finishes. Different aspects of the tribocorrosion responses, such as friction coefficient, current evolutions and degradation mechanisms will be addressed in the following sections. The most relevant parameters are summarized in Table 2.

4.2.1. Evolution of the friction coefficient

Friction coefficients measured during tribocorrosion tests under potentiostatic control at both studied potentials (E_{cat} and E_{pass}) are presented in Fig. 3. One representative curve is shown for each surface state for illustrative purpose (all the tests exhibited a good reproducibility).

At 1 N (Fig. 3a), the COF values were significantly modified by the applied potential for samples SSO and SSEP. The COF was higher at E_{cat} (about 0.6) with respect to the values registered at E_{pass} (about 0.4), which is in accordance to different studies [37,39]. This positive shift of the COF under cathodic potential was attributed to surface modification, i.e. oxide layer removal, without thermodynamic conditions for repassivation. Nevertheless, for the SSM surface, the COF at E_{cat} displayed only a slight increase in comparison to E_{pass}.

The COF evolution of SSEP sample reached the steady state between 50 – 100 cycles, at both potentials and loads. While SSO surface at 1 N, under cathodic potential and for the used sliding distance, did not show the stationary state, indicating a continuous production of debris as a consequence of the oxide-oxide contact, probably associated to the higher oxygen content at the SSO surface as previously reported [34]. Nevertheless, under the other testing conditions, the SSO sample presented similar characteristics to the SSEP specimen. The COF evolution of SSM took longer times to reach the steady state (about 300 cycles) for both applied potentials at 1 N and similar behavior at E_{cat} for 5 N load. This behavior could be probably related to the topography of this sample.

It is worth mentioning that at 1 N it could be clearly observed how the surface characteristics of the studied samples (initial oxygen concentration, roughness and passivity) influenced the evolution of COF under both testing potentials.

Concerning the COF monitoring at E_{pass}, the smaller values apparently indicated that the tribological contact with the alumina counterbody was facilitated when the polarization conditions allowed the repassivation of the surface. Similar observations were provided by Sun and Rana [37], who attributed this effect to the presence of the oxide film and its increasing thickness upon polarization at a passivating potential. Such perception dates back to Tingle [50], who mentioned that the oxide films formed on metals could partially bear the applied load and provide an apparent lubrication action. This bearing effect could decrease the total shear strength of the tribological pair due to the reduction of the total contact area, thus decreasing the friction of the system.

At 5 N of normal load, the friction coefficient values presented a sensible decrease in comparison to the ones computed at 1 N, for all samples and both potentials. Under cathodic control the steady state was reached only for samples SSEP and SSO. However, the observed trends at 1 N were also verified at 5 N: greater values of COF at E_{cat} than at E_{pass} (for SSO and SSEP) and only minor differences recorded for SSM.

The COF values from tribocorrosion testing at E_{cat}, which was supposed as pure wear without corrosion, showed lower values than under pure wear in dry conditions (Fig. 1). This outcome pointed out the lubricating action of the NaCl solution, despite its low viscosity [51]. The COF values for samples SSO and SSEP decreased by approximately 10%, from dry to wet conditions and for both loads, while the respective decrease of COF was greater for SSM (about 50% at 1 N and about 15% at 5 N). This sharp reduction in the friction coefficient observed for SSM in the presence of aqueous electrolyte could be a sign of its enhanced tribological properties, such as reported by the materials supplier. The lubricating action of the NaCl solution could also be inferred by comparing the wear tracks morphologies in both cases (Tables 1–2), i.e. reduction of wear track widths under lubricating conditions. For instance, for SSO at 5 N, the wear track width decreased from approximately 460 µm–195 µm, from dry to wet conditions.

4.2.2. Current evolution

Prior to the tribological contact and during tribocorrosion tests, negative currents (I) were measured at cathodic potential, indicating the absence of corrosion and that the main electrochemical activity occurring was the oxygen reduction reaction. Since no corrosion was expected at E_{cat}, the material loss in NaCl electrolyte might be essentially related to the mechanical wear action under lubricating regime [37,39].

Conversely, at E_{pass}, when the tribological pair came into contact and sliding started, the positive current magnitude increased abruptly (two to four orders of magnitude) (Fig. 4). The rupture of the passive film on the tested area, enhanced the current flow through the wear track. Once the sliding contact finished, the current values rapidly decreased due to the repassivation process. Nonetheless, these values were slightly higher than those registered prior to sliding. Two factors might have played a concomitant role here. The first one is related to the morphological and mechanical changes of the surfaces as a result of the wear track formation. The second factor is the fact that after tribological contact, the passive layers formed by the application of E_{pass} were necessarily different than those exhibited by the industrially treated surfaces. The anodic (positive) currents computed throughout the anodic potentiostatic test were attributed to both the oxidation of the metal substrates and the oxidation of third body particles entrapped within the contact [52]. Average current values registered during wear are reported in Table 2 (currents measured before and after sliding were considered as negligible for further calculations).

Table 2
Summary of the tribocorrosion parateters obtained from testing at E_{pass} = +200 mV and E_{cat} = −400 mV (vs. g/AgCl/KCL$_{sat}$) for the treated 316L surfaces at 1 N and 5 N.

	Load (N)	I (µA)	V_T 10^{-3} (mm^3) +200 mV	V_{chem} 10^{-3} (mm^3) +200 mV	V_{mech} 10^{-3} (mm^3) +200 mV	$V_t = V_{mech}$ 10^{-3} (mm^3) −400 mV	Wear track width (µm) +200 mV	−400 mV	COF +200 mV	−400 mV	Hardness in wear track (GPa) +200 mV	−400 mV
SSO	1	28 ± 4	0.8 ± 0.1	0.7 ± 0.1	0.1	0.2 ± 0.1	184 ± 25	119 ± 10	0.4 ± 0.1	0.6 ± 0.1	–	–
	5	67 ± 12	2.2 ± 0.2	1.6 ± 0.3	0.6	0.9 ± 0.2	253 ± 15	194 ± 12	0.4 ± 0.1	0.4 ± 0.1	5.1 ± 0.6	3.4 ± 0.2
SSEP	1	35 ± 4	0.6 ± 0.1	0.8 ± 0.1	−0.3	0.3 ± 0.1	150 ± 13	127 ± 23	0.4 ± 0.1	0.6 ± 0.1	–	–
	5	106 ± 13	2.4 ± 0.3	2.5 ± 0.3	−0.01	0.7 ± 0.2	260 ± 10	192 ± 48	0.4 ± 0.1	0.4 ± 0.1	4.7 ± 0.4	3.7 ± 0.2
SSM	1	12 ± 8	–	0.3 ± 0.2	–	–	187 ± 58	195 ± 8	0.3 ± 0.1	0.4 ± 0.1	–	–
	5	77 ± 7	1.8 ± 0.8	1.7 ± 0.3	0.1	–	231 ± 18	230 ± 25	0.4 ± 0.1	0.4 ± 0.1	5.6 ± 0.2	5.2 ± 0.3

Fig. 3. Evolution of friction coefficient of 316L stainless steel presenting distinct surface treatments (SSO, SSEP, SSM) during tribocorrosion tests under potentiostatic control (E_{pass} = +200 mV, E_{cat} = −400 mV vs. Ag/AgCl/KCl$_{sat}$), the total testing time was about 800 s: a) E_{cat} at 1 N; b) E_{cat} at 5 N; c) E_{pass} at 1 N; d) E_{pass} at 5 N. (color online). (For interpretation of the references to color in this figure legend, the reader is referred to the Web version of this article.)

The abrupt increase of the current during sliding was observed immediately for SSO and SSEP upon contact, at both testing loads (Fig. 4). In these cases, a steady state with spiky behavior was quickly achieved, indicating the rapid disruption of the passive layers and the removal of the asperities in the contact zones. Nevertheless, the SSM sample exhibited a different behavior, with currents progressively increasing as a function of the cyclic sliding process, for both applied loads but particularly for 1 N. Here, the morphology of the peaks indicated the presence of a slight wear, demonstrating that the low I registered was representative of the limited area of tribological contact. In other words, passive layer breakdown and wear occurred locally and in progressive fashion, from the peaks of asperities down to their valleys. It is worth remembering that the higher hardness of the SSM probably favored the smaller contact area in this case. Regarding the 5 N load, wear was obviously intensified, leading to a more rapid increase of the contact area and, consequently of the current (Table 2). Thus, the current raised few minutes after the contact (about 200 cycles) and reached the steady-like state, most likely reflecting the progressive increase of the active area due to a gradual removal of the micro-undulation topography.

4.2.3. Degradation mechanisms during tribocorrosion testing

SEM observations were carried out to identify the wear mechanisms produced during tribocorrosion tests (Figs. 5–7). Moreover, optical profilometry characterization was performed on the wear tracks and alumina counterparts (Figs. 6–8). These characterizations revealed that the morphology of the wear tracks, the severity of the damage and the mechanisms were strongly modified by the applied potential (−400 mV or +200 mV vs. Ag/AgCl/KCl$_{sat}$).

Under cathodic potential at 5 N and regardless the sample, wear tracks showed traces of smoothening. Here, the asperities were probably plastically deformed and removed by shearing during sliding contact, producing debris that were deposited/compacted mainly in the edges of the wear tracks (Fig. 5). These compacted regions subsequently suffered cracking due to the fatigue process, possibly creating new wear particles that were either ejected from the contact or remained entrapped in it. Moreover, some scratches characteristic of abrasive wear observed on the SSEP and SSM surfaces, were barely detected for the SSO sample. This probably happened because of the higher Cr content in the near-surface zones (at least 10 nm down from the top-surfaces) of SSEP and SSM [34], which potentially contributed to the production of harder debris particles. In other words, the likely superior amount of chromium oxides (hard phases) was responsible for generating more abrasion on
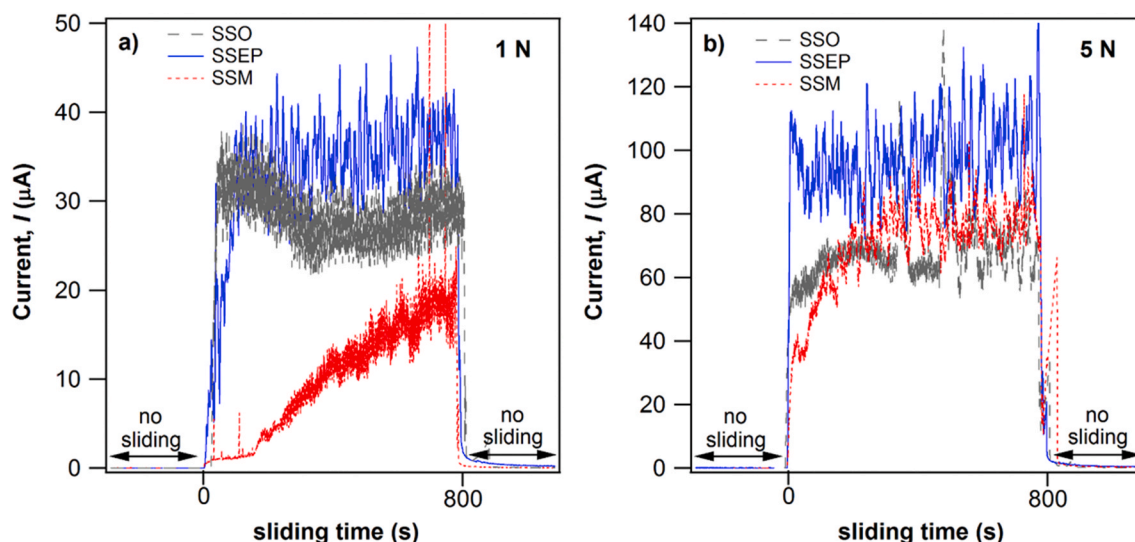
Fig. 4. Current evolution during tribocorrosion tests performed on industrial 316L samples under potentiostatic anodic polarization ($E_{pass} = +200$ mV) at: a) 1 N and b) 5 N load. The sliding time about 800 s corresponds to 800 sliding cycles. (color online). (For interpretation of the references to color in this figure legend, the reader is referred to the Web version of this article.)

SSEP/SSM than on SSO.

Regarding the 1 N load, a similar response to the one obtained at 5 N was observed for SSEP and SSO samples. Alternatively, for the resulting SSM surfaces at 1 N, the most evident features were: scratches from abrasive wear within the entire discontinuous worn zone and wear debris deposits that remained on the wear track. Again, due to the surface micro-undulation topography, more debris might have remained entrapped in the contact zone leading to further abrasive wear.

Under cathodic conditions considerable amount of wear debris were deposited and compacted on the alumina counterparts (Fig. 6) specially for the specimens SSEP and SSM at 1 N and in a higher amount at 5 N, favoring the contact 316L–316L and corroborating, therefore, the evolution of the friction coefficient with the sliding distance reported above (Fig. 3).

EDS analysis performed on the worn surfaces (Fig. 5) tested under cathodic control, revealed the accumulation of oxides in the wear track edges as well as in the islands-like regions. These oxides were rich in Cr, indicating compaction of wear debris arising from the top surfaces in these regions. Moreover, SEM observations in backscattered mode (not presented here) exhibited that wear debris were washed away a few hundred micrometers from the wear track.

Regardless the sample, surface analysis (Fig. 5) also highlighted that pure mechanical wear damage at cathodic potential was less aggressive than wear produced in dry conditions (Fig. 2). This fact confirmed the lubrication action and the possible cooling effect of the electrolyte (probably reducing flash temperatures during contact), which reduced the adhesive wear and modified the wear mechanisms. Under wet conditions, the generated debris could be more easily ejected from the contact zone than in dry sliding, reducing the mechanical damage.

Concerning the tribocorrosion tests carried out at E_{pass} (+200 mV vs. Ag/AgCl/KCl$_{sat}$), the prevailing mechanism was abrasive wear accompanied by plastic deformation (Fig. 7), despite of the sample under study. The worn surfaces were characterized by grooves that are typical abrasion features (signaled in Fig. 7b, e, h). During the tribocorrosion process, oxide and metallic debris were produced promoting abrasive wear, *i.e.* harder oxides debris yielded more abrasion, particularly in the cases of SSEP and SSM, which presented higher Cr contents at the industrially finished surfaces. Indeed, wear tracks performed on SSEP and SSM at 1 N presented grooves in the entire worn areas, hence exhibiting more abrasion than the SSO surface, for which wear scratches were observed only at the edges of wear tracks. By increasing the normal load to 5 N (Fig. 7), a similar overall response was obtained, but with

more debris particles generation, which further induced more abrasion within the whole wear tracks in the three surfaces. The hard alumina ball counterpart clearly promoted plastic deformation and abrasive wear mechanisms since no significant adhesion of stainless steel was observed on their surfaces after the tests, as shown in the 3D optical profilometry images presented in Fig. 8. The differences with respect to the morphology of the counterparts at cathodic potential put in evidence the contrast between the mechanisms at both potentials.

With respect to E_{pass} testing, dynamic repassivation processes considerably changed the nature of the contact in comparison to results obtained at E_{cat}. In fact, by applying +200 mV, oxide layers continuously produced on the active surfaces were subsequently damaged by abrasion, leading to the generation of hard particles in the contact and modifying the extent of mechanical wear. Once oxide particles were worn out, their dissolution rate in NaCl medium was certainly lower than the dissolution rate of metallic particles eventually formed during sliding. In any case, reactive metallic debris would also undergo oxidation and further contribute to the generation of hard oxide particles, producing more abrasive wear.

The typical repassivation time for stainless steel is approximately 200 ms [37,53], while the contact interval time in the present experimental conditions was 1000 ms. Therefore, since the contact interval time was greater than the repassivation time, the worn surface areas instantaneously out of the contact would tend to repassivate during sliding wear process. One could assume that the tribological contact for tests performed at E_{pass} took place invariably in the presence of newly formed passivated layers. The dynamic nature of this process helps to understand the spiky behavior of the corresponding current curve observed in the tribocorrosion tests at E_{pass} (Fig. 4).

Complementary microscopic observations revealed the presence of small pit-like features of small diameter (less than 1 μm) in all wear tracks (Fig. 7b, e, h). These pits could also have contributed to the observed current spikes [37,54]. Although pitting was not supposed to occur at E_{pass} (lower potential than pitting potential) [34], specific tribocorrosion conditions might have triggered the development of localized corrosion. For instance, Sun and Bailey [55] explained that pitting initiation is due to the mechanical action during sliding under specific testing parameters of contact frequency, sliding time and load, which can produce passive film destruction, microcracks, voids and surface roughness increase; consequently facilitating pitting formation. In addition, the increase of these parameters produces a growth in the pits size and number up to certain critical values where the wear action
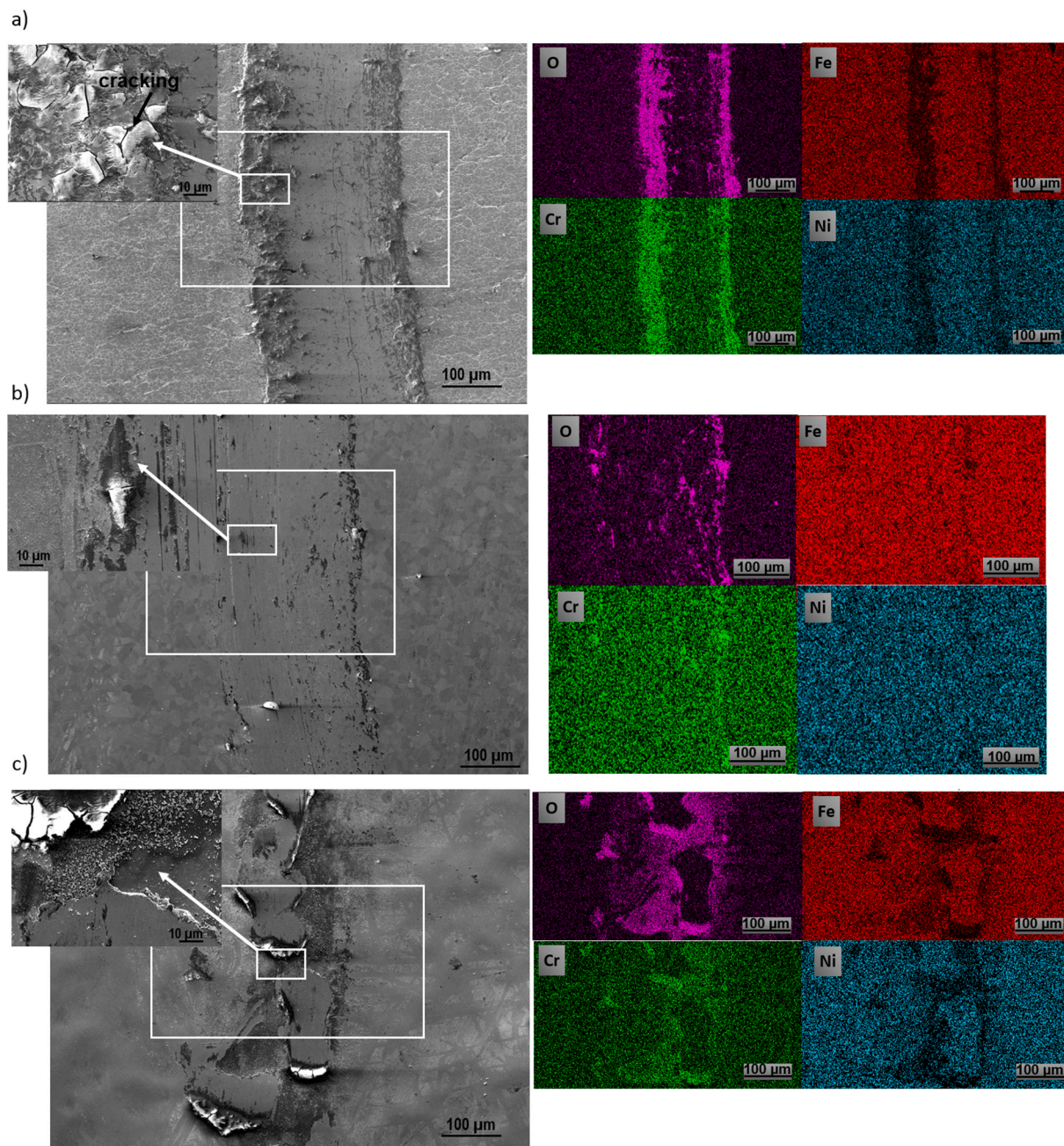
Fig. 5. SEM/EDS analysis of wear tracks obtained after tribocorrosion tests under potentiostatic cathodic polarization at 5 N load: a) SSO, b) SSEP and c) SSM. (color online). (For interpretation of the references to color in this figure legend, the reader is referred to the Web version of this article.)

surpasses the conditions for pitting development. Furthermore, besides of the described mechanical effect, the diffusion of oxygen towards the areas under tribological contact is often complicated [56]. In this case, local oxygen-depletion conditions might have lowered the pitting corrosion potential of the stainless steel, allowing the formation of pits at a potential that was initially promoting passivity [57–59]. In other words, the local breakdown of the passive film induced by Cl^- would occur at lower potentials under lower associated oxygen concentration conditions. However, the validation of this hypothesis will require further investigation.

The small pits size might be explained by the continuous competition between pit growth and wear. Pits formed on the wear tracks could be crashed between two subsequent contacts, most likely limiting their final size [55]. In contrast to classical corrosion tests, limited aggressiveness (acidity) of the solution inside the pits was expected due to the

dynamic nature of the tribocorrosion process, favoring the repassivation of initiated pits during the non-contact period. Moreover, repassivation processes after sliding explain the current reaching similar values to the ones registered at the beginning of the tests (Fig. 4), indicating the metastable character of the pits as well. This phenomenon was previously explained by Sun and Rana [37].

In any case, the formation of small pits should not modify the general kinetics of the repassivation process, since they are related to very localized phenomena of passive film breakdown. Furthermore, the contribution of pitting to the measured currents should be appreciably lower than that related to the transient exposition of fresh metallic substrates promoted by the contact.
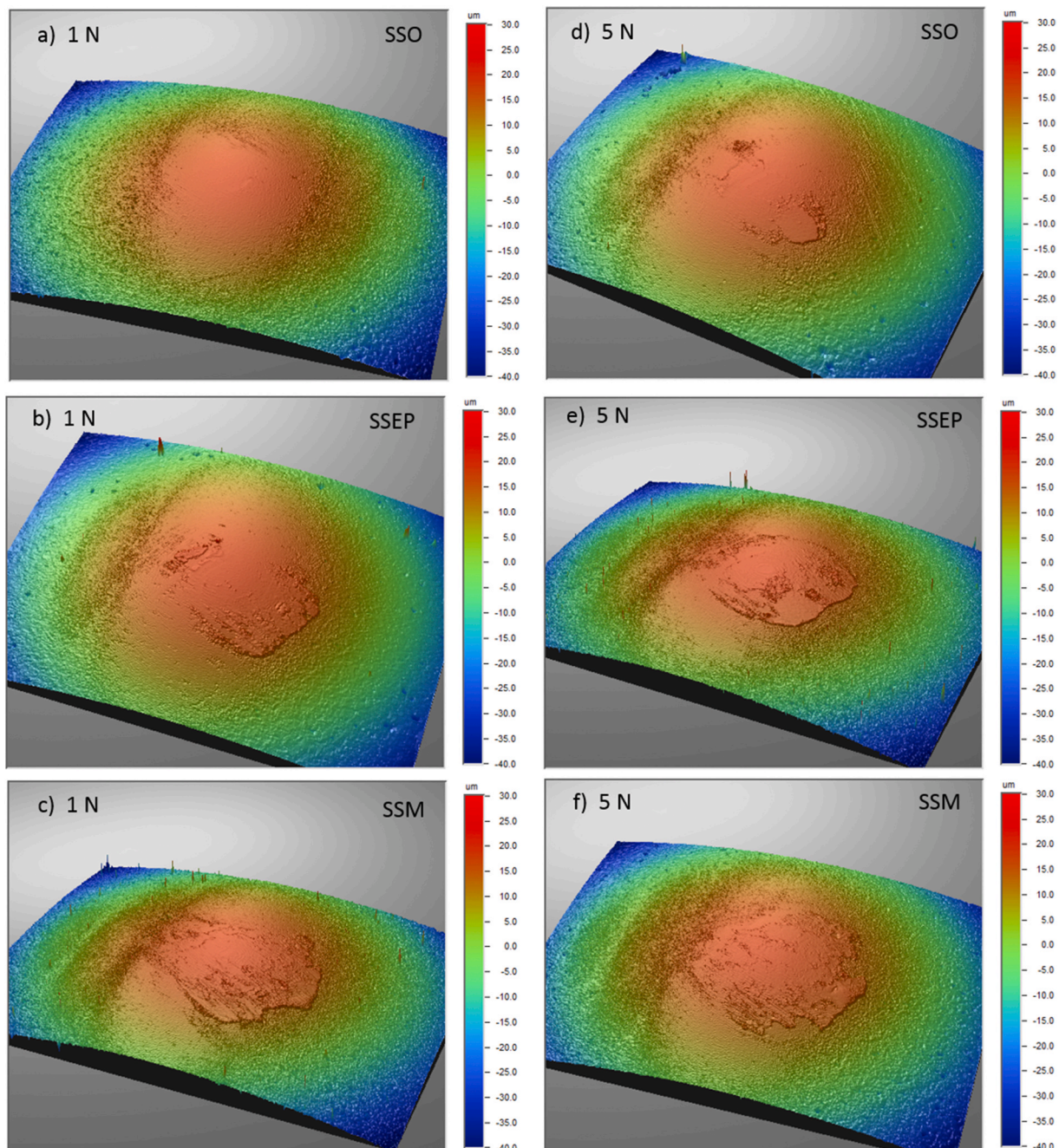
Fig. 6. 3D optical profilometry showing the topography corresponding to the alumina ball surfaces at 800 cycles (10 m) sliding distance after tribocorrosion tests under cathodic control. The corresponding samples and testing loads are indicated in the figures. (color online). (For interpretation of the references to color in this figure legend, the reader is referred to the Web version of this article.)

5. Discussion

5.1. Tribocorrosion behavior as a function of applied potential

The aforementioned results clearly indicated that the applied potential altered the tribocorrosion behavior of 316L stainless steel, regardless the surface treatment. Illustrative examples of the wear track profiles highlight the significant difference between the damage produced at both studied potentials (Fig. 9). The volume loss calculated from profilometry measurements at cathodic potential represented between 54 to 74% less of the total volume loss at passive potential, for SSO and SSEP, respectively. Similarly, SSM showed smaller worn volumes at E_{cat}, albeit the surface undulations in this case produced

discontinuities in the wear tracks that hindered the volume calculation.

The applied potential also presented a significant impact on the COF evolution determined for SSO and SSEP (Fig. 3). COF change upon applied potential was more significant at 1 N (about 40% increase from E_{pass} to E_{cat}) than at 5 N (~15% increase from E_{pass} to E_{cat}). In general, a higher value of the friction coefficient indicates greater wear and strain. However, as mentioned above, wear was less severe at E_{cat} than at E_{pass} as already reported by other authors [5,38,39]. Alternatively, the degree of wear might be related to the mechanisms of dissipation of the frictional energy and not uniquely related to the intensity of the friction force [39].

Concerning the SSM surface, differences between the COF at E_{cat} or at E_{pass} were barely observed at 1 N and were almost negligible at 5 N
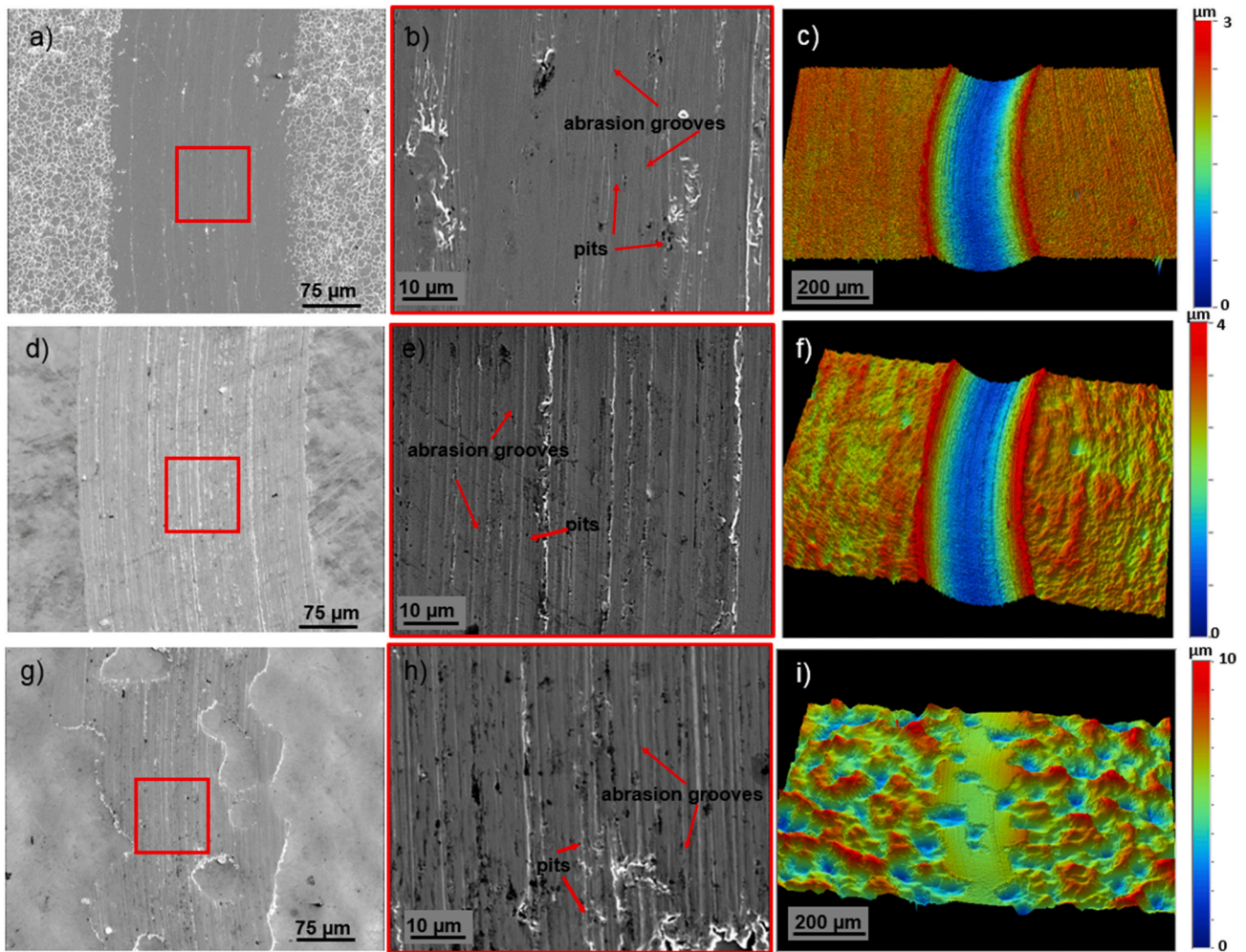
Fig. 7. SEM in secondary electron mode of wear tracks morphology obtained under E_{pass} at 5 N: a-b) SSO, d-e) SSEP, g-h) SSM; c), f) and i) 3D surface representation by optical profilometry of SSO, SSEP and SSM, respectively. (color online). (For interpretation of the references to color in this figure legend, the reader is referred to the Web version of this article.)

(less than 10% of variation). This different behavior was related to the particular SSM topography, which favored the lubrication conditions. The penetration of the electrolyte on the bottom (valleys) of regularly spaced micro-undulations probably led to mixed lubrication regime within the contact area, instead of a boundary lubrication one. This morphological effect was less relevant at E_{pass}: in this case the electro-mechanical changes induced by anodic polarization (surface oxidation) were apparently preponderant, which explained the similar COF values obtained for all the samples at +200 mV. In addition, possible effects related to the particular properties of the SSM surface (higher hardness and twinned microstructure [34]) could not be discarded of having played a role during tribocorrosion tests [16,32].

The dissimilar response at both potentials could be associated to the modification of the alloy resistance against mechanical wear and the facilitation of wear-accelerated corrosion according to the applied potential, such as reported by Favero et al. [39]. Similarly, Bidiville et al. [38] mentioned that the applied potential influenced the surface plastic behavior of 316L steel against alumina ball during sliding. They found that the near surface exhibits a more strained structure with smaller grains and strain induced martensite at the passive potential. Here, the difference in the deformation response is probably related to the passive film that could act as a dislocation source in the underlying metal and also as a barrier against dislocation annihilation at the surface [60]. At passive potential, the strain accumulated at the surface likely generates three-dimensional defects such as micro-voids and α-martensite,

facilitating the nucleation of cracks and produce the detachment of particles and more wear [38]. This could explain the increase of the total wear of the studied 316L samples at anodic potential. Conversely, at cathodic potential, since the passive layer could not repassivate, dislocations might be annihilated, reducing their accumulation in the metal [38], and, therefore, creating less defects and making the surface more resistant to wear.

It is important to mention that the surface hardness, after polarization at both potentials increased (Table 2) with respect to the hardness of fresh substrates [34]. This was true for all surface treatments and work hardening was the most likely cause. Additionally, hardness values were greater at samples subjected to anodic (passive) potential in comparison to those subjected to cathodic potential. As established by previous investigations [38,39], microstructural changes and work hardening are more severe at anodic potentials; as a result of complex mechanisms, as described above. The decrease of hardness between anodic values and cathodic ones was about 20–30% for samples SSO and SSEP, and about 8% for SSM.

5.2. Material damage during tribocorrosion

During tribocorrosion tests under anodic polarization, the chemical wear component represented the main contribution for the three surfaces (Fig. 10). Thus, the material loss ascribed to corrosion accelerated by wear action was more significant than the mechanical wear
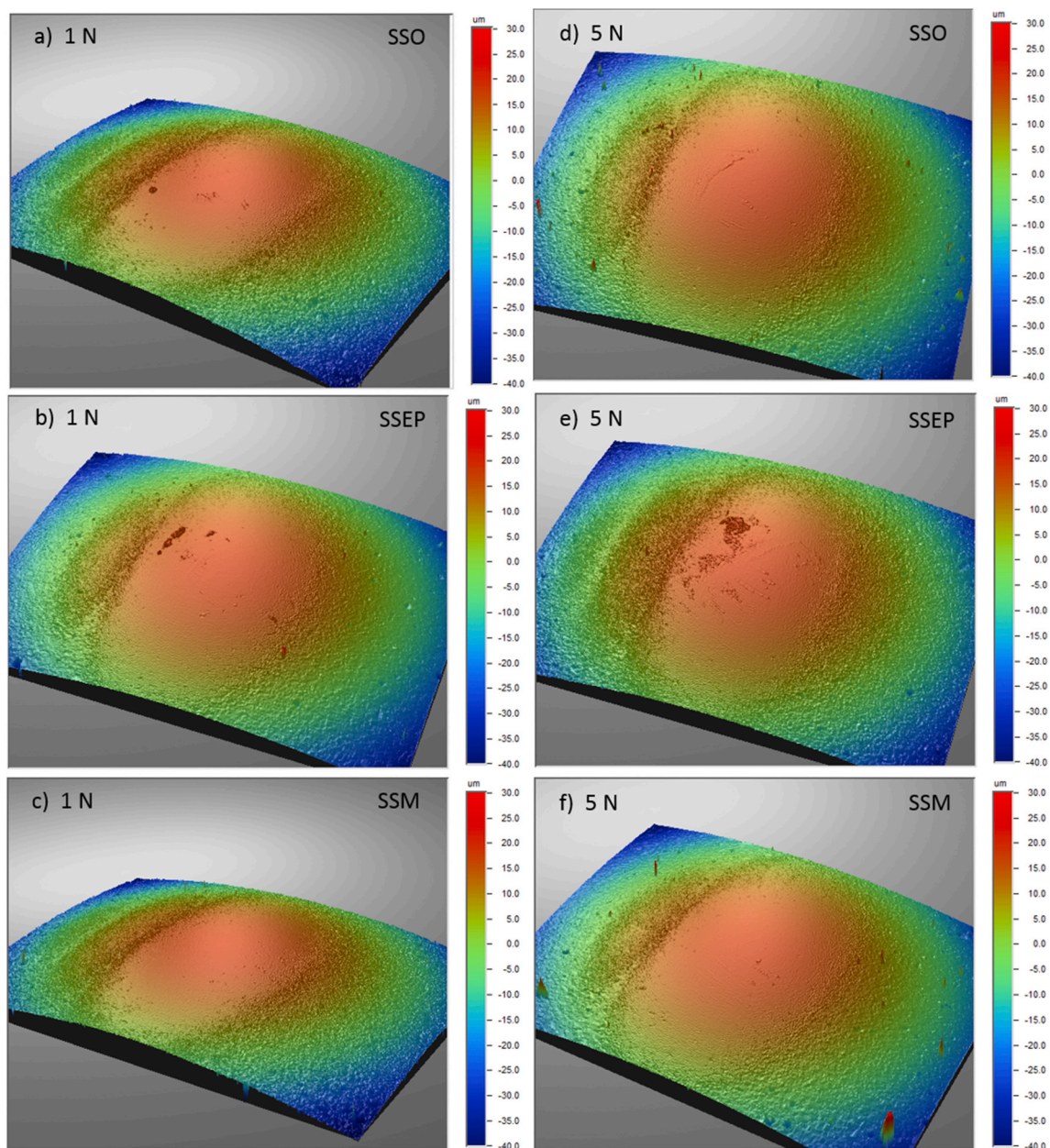
Fig. 8. 3D optical profilometry showing the topography corresponding to the alumina ball surfaces at 800 cycles (10 m) sliding distance after tribocorrosion tests under anodic control. The corresponding samples and testing loads are indicated in the figures. (color online). (For interpretation of the references to color in this figure legend, the reader is referred to the Web version of this article.)

component (Eq. (1)), which represented only a small contribution of the total material loss. Nonetheless, it is worth mentioning that both components were related to important uncertainties that could have led to small miscalculations, such as: overestimation of V_{ch} (e.g. oxidation valence, contributions of the small pits or debris oxidation to the measured current); and underestimation of V_t (*e.g.* post-mortem characterization of wear tracks; wear debris adhered to the contact zones).

Considering the SSM sample, the total wear volume (V_t) was only estimated under E_{pass} (at 5 N). The limited wear observed under E_{cat} (or under E_{pass} at 1 N) combined with its topography rendered the measurement of wear track profiles too uncertain. However, it could be easily inferred that the total wear volume was smaller than the values obtained for SSO and SSEP.

The total loss volume logically increased with the applied load (1 and 5 N) during the tribocorrosion tests, as a consequence of the contact area and chemical wear growth at E_{pass}. Landolt et al. [3] described a

proportional relationship between the repassivation current and the applied force, implicating that higher loads would produce more chemical wear. This proportional relation is also valid for the mechanical wear component that generally follows the Archard's law (when neglecting third body effects).

As expected, a different tribocorrosion behavior was obtained for the three surfaces under study, particularly at E_{pass}. The SSEP surface presented a detrimental tribocorrosion response in comparison with the SSO and SSM ones, indicating the important role of topography and chemical composition of the contacting surfaces as reported also by Landolt et al. [61].

The highest chemical wear obtained for SSEP under both loads was probably associated to different factors. Firstly, the initial chemical composition and mechanical properties of the passive layer [34]. Second, the structure of the passive layer, which was certainly different after electropolishing, since the film growth is very sensitive to the
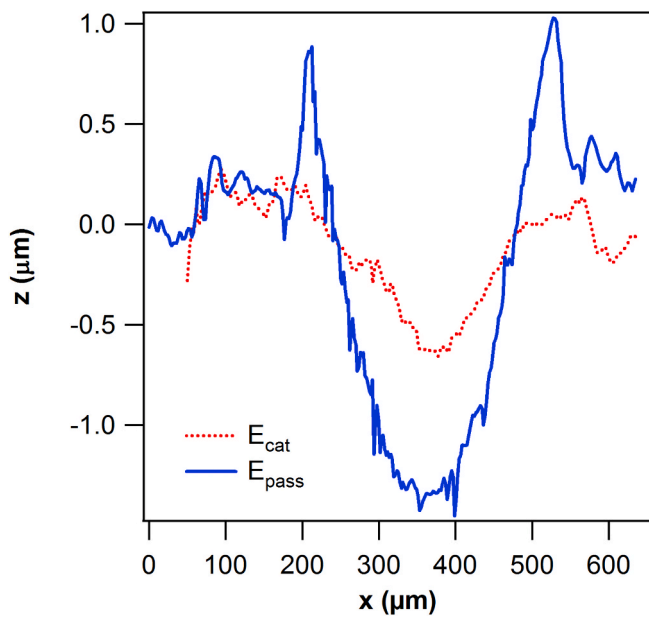
Fig. 9. Wear track profiles obtained by optical profilometry from SSEP surfaces after tribocorrosion testing at 5 N under potentiostatic control (E_{cat} or E_{pass}). (color online). (For interpretation of the references to color in this figure legend, the reader is referred to the Web version of this article.)
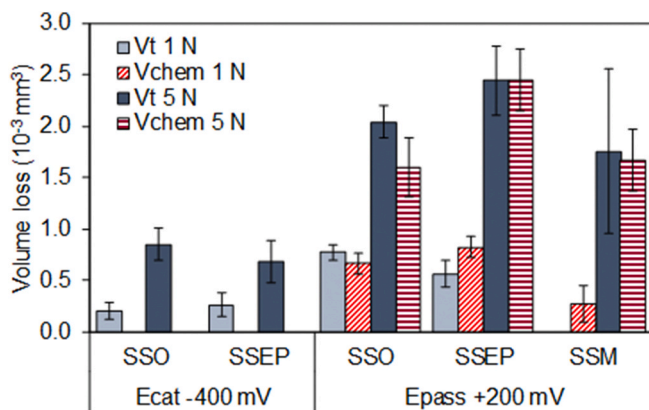
Fig. 10. Volume loss after tribocorrosion tests performed under potentiostat polarization (E_{cat} and E_{pass}) at two normal loads (1 N and 5 N). (color online). (For interpretation of the references to color in this figure legend, the reader is referred to the Web version of this article.)

formation conditions (temperature, pH, media, etc.) [62]. During electropolishing, anodic dissolution takes place and leads to faceting [63] and the passive film grows following the grain orientation, giving the microstructure reported for SSEP [34]. On the contrary, the oxide film of SSO results from a combination of steps according to the 2B surface finish [35]. These previous factors, chemical composition, mechanical properties and structure of the passive film alter its mechanical behavior [10], specifically the film adhesion. A poorer adhesion of the passive film would imply its easier removal from the contact zone under load. For instance, indentation results reported previously [34] indicated that the passive layer of SSEP exhibited cracking, which was highlighted by the presence of pop-in on the load-displacement curves. Finally, the extent of accumulated deformation during wear was likely more significative in the electropolished surface, favoring the corrosion process. As mentioned by Li and Li [64], the increase of dislocation density due to plastic deformation and strain intensifies the corrosion rate by providing more active sites for the electrons.

Conversely to the electropolishing treatment, the micro-undulation process (SSM) ameliorated the tribocorrosion response. The micro-undulated topography definitely affected the depassivation/repassivation processes and mechanical wear rates. This behavior was consistent with the known model proposed by Mischler et al. [4] (Eq. (3)), which describes the anodic current I_p in the wear track as follows:

$$I_p = kvQ_p \left(\frac{F}{H}\right)^{0.5} \tag{3}$$

where k includes a proportionality factor related to the probability of depassivation and the number of contact asperities, v is the sliding velocity, Q_p is the anodic charge needed for repassivation, F is the normal load and H is the material hardness.

Indeed, the specific topography of SSM reduced the aggressiveness of the contact: the limited real contact area imposed by micro-asperities regularly distributed decreased the k factor. As a consequence, due to the enhanced surface lubrication and a possible mixed lubrication regime [6], the effective applied load on SSM was also minor (in comparison to SSO and SSEP). Besides, high surface hardness, such as determined for SSM due to extensive plastic deformation induced by micro-undulation, is reported to improve the general tribocorrosion behavior [32]. This better tribocorrosion behavior might also be related to the twining associated to the micro-undulated surface, reported so as to improve the corrosion response [17,65]. In general, the described characteristics helped to improve the tribocorrosion response of 316L stainless steel treated by micro-undulation. It is worth mentioning that with increasing loads and/or with continuous sliding overtime, the benefits of the micro-undulation treatment progressively vanish as a result of severe surface modifications.

6. Conclusions

- The dry wear sliding behavior of the 316 stainless steel plates under study was dominated by adhesive wear and it was not significantly modified by the industrial finishing treatments.
- The tribocorrosion response of the treated surfaces was modified by the applied potential producing a more aggressive response under anodic polarization (+200 mV vs. Ag/AgCl/KCl$_{sat}$), regardless the surface treatment. The tribocorrosion response was demonstrated to be dominated by the chemical wear component.
- Hardness increase in the wear tracks produced by tribocorrosion was related to microstructural modifications and work hardening. This effect was more predominant at passive potential, as demonstrated by nanoindentation analysis. The formation of passive layers was responsible for this behavior, as a result of the dynamic process of depassivation/repassivation, in which complex mechanisms interfere.
- The industrial electropolishing treatment (SSEP) produced a detrimental effect on the tribocorrosion behavior in NaCl media at anodic potential in comparison with the SSO treatment. This response was related to diverse possible causes: debris resulting from a surface richer in Cr (more abrasion), the mechanical behavior of the initial passive layer (adhesion) and the higher extent of accumulated deformation (more active zone for corrosion).
- The micro-undulation process (SSM) enhanced the tribocorrosion response. The improvement was principally accounted to the surface topography (improved lubrication) and to the superior surface hardness (reduction of mechanical wear).

CRediT authorship contribution statement

Stephania Kossman: Conceptualization, Methodology, Formal analysis, Writing - original draft, Investigation, Validation, Visualization. **Leonardo B. Coelho:** Conceptualization, Methodology, Validation, Investigation, Writing - original draft, Visualization. **Alberto**

Appendix A. Supplementary data

Supplementary data to this article can be found online at https://doi.org/10.1016/j.wear.2020.203341.

References

[1] J.-P. Celis, P. Ponthiaux, European Federation of Corrosion., Testing tribocorrosion of passivating materials supporting research and industrial innovation : handbook, Maney Pub, 2012 (accessed December 2, 2019), https://books.google.fr/books?id=QzkrDwAAQBAJ.

[2] D. Landolt, S. Mischler, Tribocorrosion of passive metals and coatings, Woodhead Publishing, Cambridge, UK, 2011, https://doi.org/10.1533/9780857093738.

[3] D. Landolt, S. Mischler, M. Stemp, Electrochemical methods in tribocorrosion: a critical appraisal, Electrochim. Acta 46 (2001) 3913–3929, https://doi.org/10.1016/S0013-4686(01)00679-X.

[4] S. Mischler, S. Debaud, D. Landolt, Wear-accelerated corrosion of passive metals in tribocorrosion systems, J. Electrochem. Soc. 145 (1998) 750–758, https://doi.org/10.1149/1.1838341.

[5] S. Guadalupe Maldonado, S. Mischler, M. Cantoni, W.J. Chitty, C. Falcand, D. Hertz, Mechanical and chemical mechanisms in the tribocorrosion of a Stellite type alloy, Wear 308 (2013) 213–221, https://doi.org/10.1016/j.wear.2013.04.007.

[6] S. Cao, S. Guadalupe Maldonado, S. Mischler, Tribocorrosion of passive metals in the mixed lubrication regime: theoretical model and application to metal-on-metal artificial hip joints, Wear 324–325 (2015) 55–63, https://doi.org/10.1016/j.wear.2014.12.003.

[7] V.I. Pokhmurs'Kyi, V.M. Dovhunyk, Tribocorrosion of stainless steels (Review), Mater. Sci. 46 (2010) 87–96, https://doi.org/10.1007/s11003-010-9267-3.

[8] K. Asami, K. Hashimoto, An X-ray photo-electron spectroscopic study of surface treatments of stainless steels, Corrosion Sci. 19 (1979) 1007–1017, https://doi.org/10.1016/S0010-938X(79)80091-8.

[9] A. Pardo, M.C. Merino, A.E. Coy, F. Viejo, R. Arrabal, E. Matykina, Effect of Mo and Mn additions on the corrosion behaviour of AISI 304 and 316 stainless steels in H2SO4, Corrosion Sci. 50 (2008) 780–794, https://doi.org/10.1016/j.corsci.2007.11.004.

[10] R.S. Yassar, L. Scudiero, A.S. Alamr, D.F. Bahr, M.G. Norton, Microstructure-mechanical and chemical behavior relationships in passive thin films, Thin Solid Films 518 (2010) 2757–2763, https://doi.org/10.1016/j.tsf.2009.08.032.

[11] A. Alamr, D.F. Bahr, M. Jacroux, Effects of alloy and solution chemistry on the fracture of passive films on austenitic stainless steel, Corrosion Sci. 48 (2006) 925–936, https://doi.org/10.1016/j.corsci.2005.02.018.

[12] M.B. Leban, Č. Mikyška, T. Kosec, B. Markoli, J. Kovač, The effect of surface roughness on the corrosion properties of type AISI 304 stainless steel in diluted NaCl and urban rain solution, J. Mater. Eng. Perform. 23 (2014) 1695–1702, https://doi.org/10.1007/s11665-014-0940-9.

[13] S.D. David Tabor, Friction, lubrication, and wear, in: H. Rothbart, T.H. Brown (Eds.), Mech. Des. Handbook, Meas. Anal. Control Dyn. Syst., second ed., McGraw-Hill Education, New York, 2006, p. 900.

[14] G.T. Burstein, S.P. Vines, Repetitive nucleation of corrosion pits on stainless steel and the effects of surface roughness, J. Electrochem. Soc. 148 (2001) B504–B516, https://doi.org/10.1149/1.1416503.

[15] A. Latifi, M. Imani, M.T. Khorasani, M.D. Joupari, Electrochemical and chemical methods for improving surface characteristics of 316L stainless steel for biomedical applications, Surf. Coating. Technol. 221 (2013) 1–12, https://doi.org/10.1016/j.surfcoat.2013.01.020.

[16] Y. Sun, Sliding wear behaviour of surface mechanical attrition treated AISI 304 stainless steel, Tribol. Int. 57 (2013) 67–75, https://doi.org/10.1016/j.triboint.2012.07.015.

[17] T. Olugbade, J. Lu, Enhanced corrosion properties of nanostructured 316 stainless steel in 0.6 M NaCl solution, J. Bio- Tribo-Corrosion. 5 (2019) 38, https://doi.org/10.1007/s40735-019-0235-7.

[18] Electropolishing vs, Passivation – choosing the right finish, Birmingham Fasten, 2018. https://www.bhamfast.com/electropolishing-passivation/ (accessed November 19, 2019).

[19] ASTM A380/A380M - 17 standard practice for cleaning, descaling, and passivation of stainless steel parts, equipment, and systems. https://doi.org/10.1520/A0380_A0380M-17, 2017.

[20] ASTM A967/A967M - 17 standard specification for chemical passivation treatments for stainless steel parts. https://doi.org/10.1520/A0967_A0967M-17, 2017.

[21] A.P. Abbott, G. Capper, K.J. McKenzie, A. Glidle, K.S. Ryder, Electropolishing of stainless steels in a choline chloride based ionic liquid: an electrochemical study with surface characterisation using SEM and atomic force microscopy, Euro Inox, Brussels, 2006, https://doi.org/10.1039/b607763n.

[22] K. Popov, B. Grgur, S.S. Djokić, Fundamental aspects of electrometallurgy, Kluwer Academic Publishers, New York, NY, USA, 2002, https://doi.org/10.1007/b118178.

[23] Understanding the cost (and value) of electropolishing, Electro-Glo Distrib, 2019. https://www.electro-glo.com/understanding-the-cost-and-value-of-electropolishing/. accessed November 19, 2019.

[24] D. Gallitelli, D. Retraint, E. Rouhaud, Comparison between conventional shot peening (SP) and surface mechanical attrition treatment (SMAT) on a titanium alloy, Adv. Mater. Res. 996 (2014) 964–968. https://doi.org/10.4028/www.scientific.net/AMR.996.964.

[25] A. Heydari Astaraee, R. Miresmaeili, S. Bagherifard, M. Guagliano, M. Aliofkhazraei, Incorporating the principles of shot peening for a better understanding of surface mechanical attrition treatment (SMAT) by simulations and experiments, Mater. Des. 116 (2017) 365–373, https://doi.org/10.1016/j.matdes.2016.12.045.

[26] T. Balusamy, T.S.N. Sankara Narayanan, K. Ravichandran, I.S. Park, M.H. Lee, Influence of surface mechanical attrition treatment (SMAT) on the corrosion behaviour of AISI 304 stainless steel, Corrosion Sci. 74 (2013) 332–344, https://doi.org/10.1016/j.corsci.2013.04.056.

[27] A.Y. Chen, W.F. Hu, D. Wang, Y.K. Zhu, P. Wang, J.H. Yang, X.Y. Wang, J.F. Gu, J. Lu, Improving the intergranular corrosion resistance of austenitic stainless steel by high density twinned structure, Scripta Mater. 130 (2017) 264–268, https://doi.org/10.1016/j.scriptamat.2016.11.032.

[28] S.J. Lee, J.J. Lai, The effects of electropolishing (EP) process parameters on corrosion resistance of 316L stainless steel, J. Mater. Process. Technol. 140 (2003) 206–210, https://doi.org/10.1016/S0924-0136(03)00785-4.

[29] L.R. Hilbert, D. Bagge-Ravn, J. Kold, L. Gram, Influence of surface roughness of stainless steel on microbial adhesion and corrosion resistance, Int. Biodeterior. Biodegrad. 52 (2003) 175–185, https://doi.org/10.1016/S0964-8305(03)00104-5.

[30] S. Geng, J. Sun, L. Guo, Effect of sandblasting and subsequent acid pickling and passivation on the microstructure and corrosion behavior of 316L stainless steel, Mater. Des. 88 (2015) 1–7, https://doi.org/10.1016/j.matdes.2015.08.113.

[31] Z.B. Zheng, Y.G. Zheng, Effects of surface treatments on the corrosion and erosion-corrosion of 304 stainless steel in 3.5% NaCl solution, Corrosion Sci. 112 (2016) 657–668, https://doi.org/10.1016/j.corsci.2016.09.005.

[32] Y. Sun, R. Bailey, Improvement in tribocorrosion behavior of 304 stainless steel by surface mechanical attrition treatment, Surf. Coating. Technol. 253 (2014) 284–291, https://doi.org/10.1016/j.surfcoat.2014.05.057.

[33] M. Quaghebeur, Micro-undulation | Packo inox-surface treatment. https://www.electropolish.be/en/surface-treatments/per-surface-treatment/micro-ondulation accessed December 2, 2019.

[34] L.B. Coelho, S. Kossman, A. Mejias, X. Noirfalise, A. Montagne, A. Van Gorp, M. Poorteman, M.-G. Olivier, Mechanical and corrosion characterization of industrially treated 316L stainless steel surfaces, Surf. Coating. Technol. (2019) 125175, https://doi.org/10.1016/j.surfcoat.2019.125175.

[35] A01 Committee, ASTM A480/A480M-18a, standard specification for general requirements for flat-rolled stainless and heat-resisting steel plate, Sheet, and Strip, West Conshohocken, PA, 2018, https://doi.org/10.1520/A0480_A0480M-18A.

[36] 2B, 2D and cold rolled finishes. https://www.assda.asn.au/technical-info/surface-finishes/2b-2d-and-ba-cold-rolled-finishes accessed July 29, 2019.

[37] Y. Sun, V. Rana, Tribocorrosion behaviour of AISI 304 stainless steel in 0.5 M NaCl solution, Mater. Chem. Phys. 129 (2011) 138–147, https://doi.org/10.1016/j.matchemphys.2011.03.063.

[38] A. Bidiville, M. Favero, P. Stadelmann, S. Mischler, Effect of surface chemistry on the mechanical response of metals in sliding tribocorrosion systems, Wear 263 (2007) 207–217, https://doi.org/10.1016/j.wear.2007.01.066.

[39] M. Favero, P. Stadelmann, S. Mischler, Effect of the applied potential of the near surface microstructure of a 316L steel submitted to tribocorrosion in sulfuric acid, J. Phys. D Appl. Phys. 39 (2006) 3175–3183, https://doi.org/10.1088/0022-3727/39/15/S07.

[40] H.H. Uhlig, Mechanism of fretting corrosion, J. Appl. Mech. 76 (1954) 401–407.

[41] B. Bhushan, Introduction to tribology, second ed., John Wiley & Sons, Ltd, Chichester, UK, 2013 https://doi.org/10.1002/9781118403259.

[42] F.P. Bowden, D. Tabor, The Friction and Lubrication of Solids, Clarendon Press, 2001.

[43] J. Takadoum, C. Roques-Carmes, Influence of the oxidation activity of metals on friction and wear of ceramic-metal systems, Surf. Coating. Technol. 52 (1992) 153–158, https://doi.org/10.1016/0257-8972(92)90041-8.

[44] J.F. Archard, The temperature of rubbing surfaces, Wear 2 (1959) 438–455, https://doi.org/10.1016/0043-1648(59)90159-0.

[45] P.N. Bogdanovich, D.V. Tkachuk, Temperature distribution over contact area and "hot spots" in rubbing solid contact, Tribol. Int. 39 (2006) 1355–1360, https://doi.org/10.1016/j.triboint.2005.10.008.

[46] F.H. Stott, High-temperature sliding wear of metals, Tribol. Int. 35 (2002) 489–495, https://doi.org/10.1016/S0301-679X(02)00041-5.

[47] J. Jiang, M.M. Stack, Modelling sliding wear: from dry to wet environments, Wear 261 (2006) 954–965, https://doi.org/10.1016/j.wear.2006.03.028.

[48] M.H. Staia, E.S. Puchi Cabrera, A. Iost, A. Zairi, S. Belayer, A. Van Gorp, Tribological response of AA 2024-T3 aluminium alloy coated with a DLC duplex coating, Tribol. Int. 85 (2015) 74–87, https://doi.org/10.1016/J.TRIBOINT.2014.12.007.

[49] J.F. Archard, Contact and rubbing of flat surfaces, J. Appl. Phys. 24 (1953) 981–988, https://doi.org/10.1063/1.1721448.

[50] E.D. Tingle, The importance of surface oxide films in the friction and lubrication of metals. Part I. - the dry friction of surfaces freshly exposed to air, Trans. Faraday Soc. 46 (1950) 93–102, https://doi.org/10.1039/TF9504600093.

[51] J. Kestin, H.E. Khalifa, R.J. Correia, Tables of the dynamic and kinematic viscosity of aqueous NaCl solutions in the temperature range 20–150 °C and the pressure range 0.1–35 MPa, J. Phys. Chem. Ref. Data 10 (1981) 71–88, https://doi.org/10.1063/1.555641.

[52] D. Landolt, S. Mischler, M. Stemp, S. Barril, Third body effects and material fluxes in tribocorrosion systems involving a sliding contact, Wear 256 (2004) 517–524, https://doi.org/10.1016/S0043-1648(03)00561-1.

[53] J. Jiang, M.M. Stack, A. Neville, Modelling the tribo-corrosion interaction in aqueous sliding conditions, Tribol. Int. 35 (2002) 669–679, https://doi.org/10.1016/S0301-679X(02)00058-0.

[54] G.O. Ilevbare, G.T. Burstein, Role of alloyed molybdenum in the inhibition of pitting corrosion in stainless steels, Corrosion Sci. 43 (2001) 485–513, https://doi.org/10.1016/S0010-938X(00)00086-X.

[55] Y. Sun, R. Bailey, Effect of sliding conditions on micropitting behaviour of AISI 304 stainless steel in chloride containing solution, Corrosion Sci. 139 (2018) 197–205, https://doi.org/10.1016/j.corsci.2018.05.004.

[56] J.W. Oldfield, W.H. Sutton, Crevice corrosion of stainless steels: I. A Mathematical model, Br. Corrosion J. 13 (1978) 13–22, https://doi.org/10.1179/000705978798358671.

[57] R. Fratesi, Statistical estimate of the pitting potential of AISI 316L stainless steel in 3. 5% NaCl measured by means of two electrochemical methods, Corrosion 41 (1985) 114–117, https://doi.org/10.5006/1.3581972.

[58] M. Cabrini, S. Lorenzi, T. Pastore, S. Pellegrini, M. Burattini, R. Miglio, Study of the corrosion resistance of austenitic stainless steels during conversion of waste to biofuel, Materials (Basel) 10 (2017) 1–14, https://doi.org/10.3390/ma10030325.

[59] T. Prošek, P. Novák, Initiation and propagation of stainless steel pitting corrosion under heat flux, Mater. Corros. 54 (2003) 933–939, https://doi.org/10.1002/maco.200303760.

[60] T.Y. Zhang, C.F. Qian, Interaction of a screw dislocation with a thin-film-covered mode III crack, Acta Mater. 44 (1996) 4513–4520, https://doi.org/10.1016/1359-6454(96)00066-3.

[61] D. Landolt, Electrochemical and materials aspects of tribocorrosion systems, J. Phys. D Appl. Phys. 39 (2006) 3121–3127, https://doi.org/10.1088/0022-3727/39/15/S01.

[62] C.O.A. Olsson, D. Landolt, Passive films on stainless steels—chemistry, structure and growth, Electrochim. Acta 48 (2003) 1093–1104, https://doi.org/10.1016/S0013-4686(02)00841-1.

[63] D. Landolt, Fundamental aspects of electropolishing, Electrochim. Acta 32 (1987) 1–11, https://doi.org/10.1016/0013-4686(87)87001-9.

[64] W. Li, D.Y. Li, Variations of work function and corrosion behaviors of deformed copper surfaces, Appl. Surf. Sci. 240 (2005) 388–395, https://doi.org/10.1016/j.apsusc.2004.07.017.

[65] A.Q. Lu, Y. Zhang, Y. Li, G. Liu, Q.H. Zang, C.M. Liu, Effect of nanocrystalline and twin boundaries on corrosion behavior of 316L stainless steel using SMAT, Acta Metall. Sin. (English Lett. 19 (2006) 183–189, https://doi.org/10.1016/S1006-7191(06)60042-2.